

Tire Standing Wave Simulation by 3-D Explicit Finite Element Method

Jung-Chul An¹, Jin-Rae Cho¹

Summary

Tire standing wave is one of the crucial factors that may lead to unexpected tire structural failure because the total strain energy of the tire dramatically increases when it occurs. However, its analytical analysis has been limited owing not only to the complicated tire structure and material composition, but also to the problem nonlinearity. In this paper, its characteristics are numerically investigated with the help of the transient dynamic rolling analysis of the 3-D patterned tire model.

Introduction

When an inflated tire rolls on the ground above some critical speed, it shows a wave-like deformation in the circumferential direction near and behind the tire contact region. This wavy deformation called the *standing wave* starts at the leading edge of the contact patch and spreads out to the region far behind the contact patch with the increase of the rolling speed [1]. The occurrence of the standing wave accompanies the abrupt increase of the total strain energy, the heat generation rate and the rolling resistance of the tire, so that not only the fuel economy decreases considerably, but also the tire reaches structural failure within minutes. Owing to this detrimental feature, both the understanding of the standing wave and the prediction of its critical speed have been an important research subject in the tire mechanics community for several decades [2].

This study intends to investigate the standing wave using 3-D patterned tire models in which the detailed tread blocks and the complex material composition are fully considered. In the current study, the critical speed is measured at the time when the lateral deformation produces a standing wave with a wavelength. The damping effect is taken into consideration in a mass-proportional manner with the damping coefficient that was justified from the comparison with the experiments [3]. The numerical accuracy is assessed from the comparison with the experimental results and those predicted with a simple tire model.

Tire Standing Wave

Referring to Fig. 1(a) showing a typical radial pneumatic tire, the overall stiffness and mass of a tire are definitely influenced by the pattern of tread blocks and grooves, the numerical accuracy of traditional simple tire models is highly questionable, particularly for the vibration analysis. Fortunately, thanks to the advances in modeling technologies and computer facilities, the patterned tire models in which detailed tread blocks and grooves are fully considered are [4] being

¹School of Mechanical Engineering, Pusan National University, Busan 609-735, Korea

introduced nowadays. Fig. 1(b) depicts the experiment of the standing wave phenomenon, where a real tire on the rigid drum is forced to rotate up to the desired speed from a stationary position. A CCD camera-video system captures the tire shapes at various rotating speeds, and the captured digital images are examined frame by frame for the inspection of the standing wave.

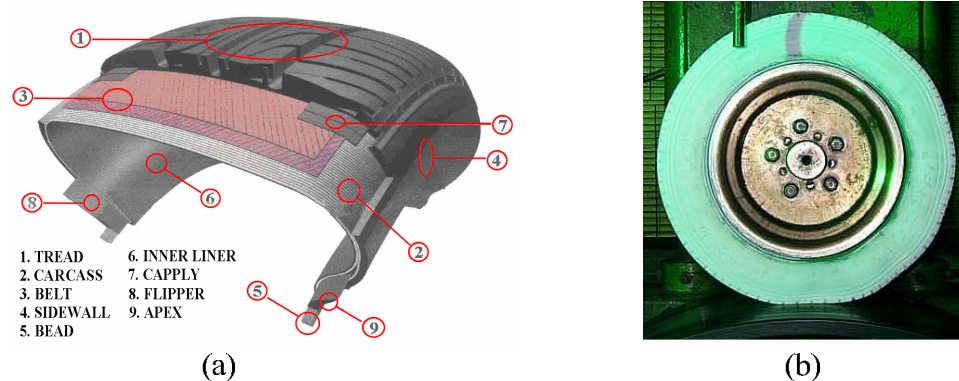


Figure 1: Radial tire. (a) structural composition, (b) standing wave experiment.

Standing waves start to form near the leading edge of the contact region once the rolling speed reaches some critical value, and extend to the region far behind the trailing contact edge as the rotating speed increases further. Of course, this extension accompanies the increase of the amplitude and wavelength of standing waves and the temperature of the tire. Traditionally, standing waves had been thought to be caused by shocks, resonances, or instabilities of the tire, but Chatterjee, et al. [5] reported that the formation of standing waves is not attributed to any of these. According to the analytical analysis of the nonlinear steady-state dynamic rolling of the balloon tire model, they found that the standing wave forms physically when the time scale of the tire rotation is shorter than one of the transient vibrations excited by the contact forces.

3-D Patterned Tire Model

The material composition of most tires is distinguished largely by the fiber-reinforced rubber (FRR) parts and the remaining pure rubber part. The FRR parts of the tire model considered here are composed of a single-ply polyester carcass, two steel belt layers, and several steel bead cords. In the current study, two belt layers in the underlying rubber matrix and a carcass layer shield with an inner-liner are modeled using composite shells. On the other hand, steel cords and the underlying rubber matrix in the bead region are modeled as a homogenized solid by utilizing the modified rule of mixtures.

Rubbers, except for the FRR parts, are modeled by the penalized first-order

Moonley-Rivlin model in which the strain density function is defined by

$$W(J_1, J_2, J_3; K) = C_{10}(J_1 - 3) + C_{01}(J_2 - 3) + \frac{1}{K}(J_3 - 1)^2 \quad (1)$$

where J_i are the invariants of the Green-Lagrangian strain tensor, and C_{10} and C_{01} are the rubber material constants. On the other hand, K is a sort of penalty parameter controlling the rubber incompressibility. It is clear that the incompressibility of rubber is asymptotically enforced as the penalty parameter approaches infinity, but the choice of K near 100 is usually recommended for the stable transient dynamic response with a reasonable time step size.

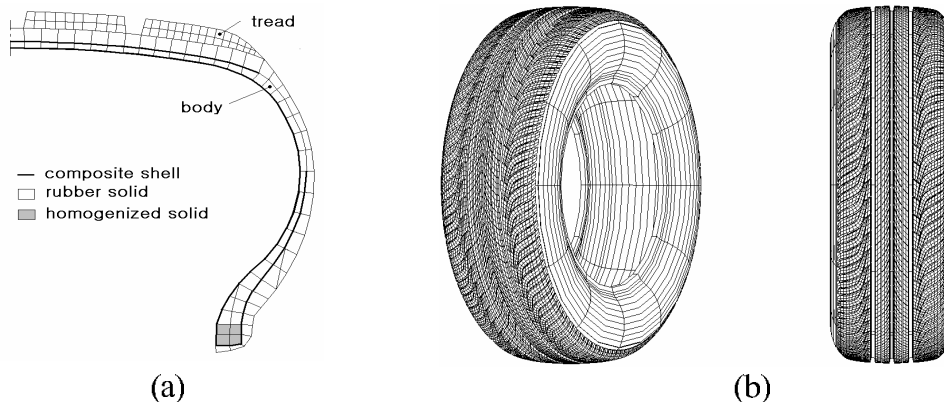


Figure 2: Tire FEM meshes. (a) 2-D section mesh, (b) 3-D patterned mesh.

Fig. 2(a) shows a 2-D section mesh that is constructed according to the above-mentioned material modeling such that pure rubber solid, composite shell and homogenized solid elements are mixed, while Fig. 2(b) represents the corresponding 3-D patterned tire mesh that is generated by our in-house program. The mesh generation of 3-D patterned tire model and the incompatible tying algorithm for combining tire body and patterned meshes are addressed in our previous paper [4].

Numerical Experiment

An automobile tire P205/60R15 with an unsymmetrical tread pattern is used for the standing wave simulation. Its patterned and simple FEM models are represented respectively in Figs. 4 and 5, where the rotating rigid drum has a radius equal to $1.7m$. The total node numbers of each tire mesh are as follows: 61,590 for the patterned tire mesh (32,754 of solid elements and 9,360 of shell elements) and 22,680 for the simple tire mesh (17,820 of solid elements and 9,180 of shell elements). On the other hand, the rigid drum is modeled with rigid elements. The tire wheel is modeled with a number of massless rigid elements connecting the tire axis with all the outer nodes of the tire bead elements that are in contact with the tire

rim. The detailed structural composition and material properties of the tire model are recorder in Table 1.

Table 1: Structural composition and material properties of tire types A and B

Item	Components			
	Carcass	Belt	Capply	Flipper
Number	2	2	2	1
Angle (°)	+88/-88	+24/-24	0/0	+25
EPI	24	20	30	22
Modulus (GPa)	4.220	110.527	1.460	1.578

Referring to Fig. 3, a standing wave simulation of the patterned tire is carried out through three sequential steps. First, the tire is inflated up to the preset internal pressure $p_i = 137.9kPa$ with the tire axis fixed. Then the bottom rigid drum is moved toward the tire by the vertical force $F_y = 475kgf$. Finally, the drum is forced to rotate clock-wise from a resting position, such that the angular velocity $\omega(t)$ of the tire increases linearly with the lapse of time. The frictional coefficient μ between the drum surface and the tire tread is set by 0.8. On the other hand, the relative bulk modulus κ/τ introduced to enforce the material incompressibility of the rubber and the penalty parameter k_p are set respectively by 100 and $10MPa$, while the damping factor c is chosen by $0.49N \cdot sec/m$.

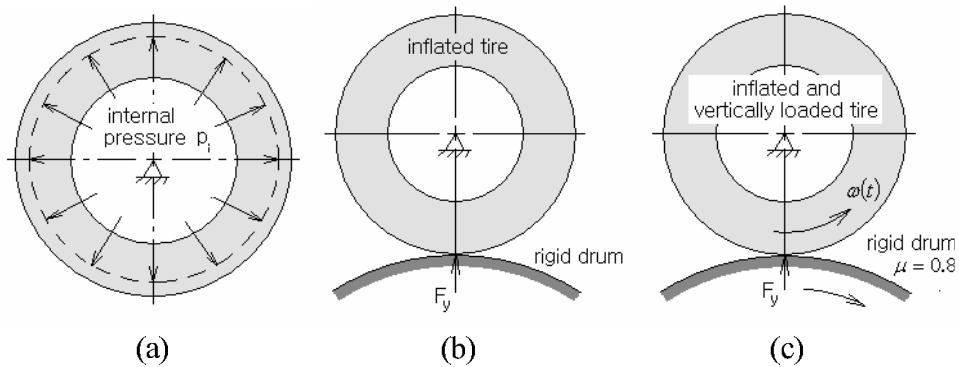


Figure 3: Three sequential steps for the standing wave simulation. (a) inflation, (b) vertical contact, (c) transient dynamic rolling.

The critical speed was measured at the time when the lateral deformation reaches the standing wave with a wavelength. Figs. 4(a) and 5(a) show the deformed configurations of both tire models at the speed before the wavy deformation forms. On the other hand, Figs. 4(b) and 5(b) show the standing waves with only a wavelength in both tire models at each critical speed. The deformed configurations of both tire models when standing waves are completely formed are represented respectively

in Figs. 4(c) and 5(c).

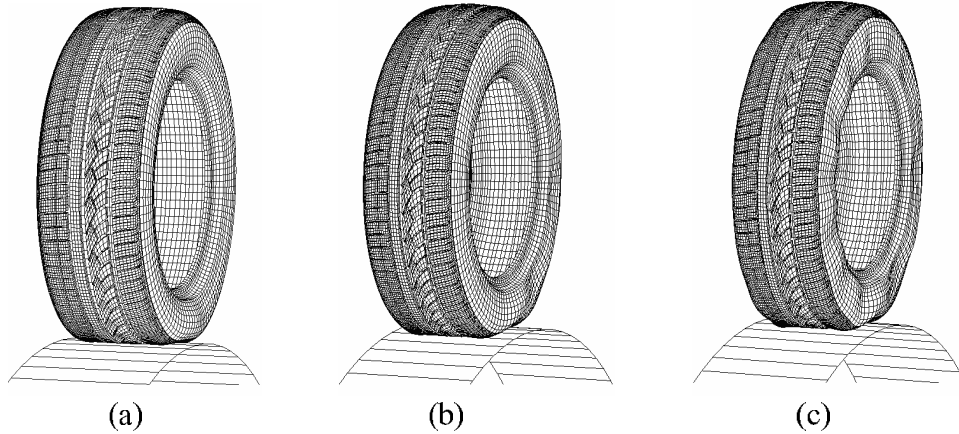


Figure 4: Patterned tire model (type A). (a) 160km/h, (b) 182km/h, (c) 220km/h.

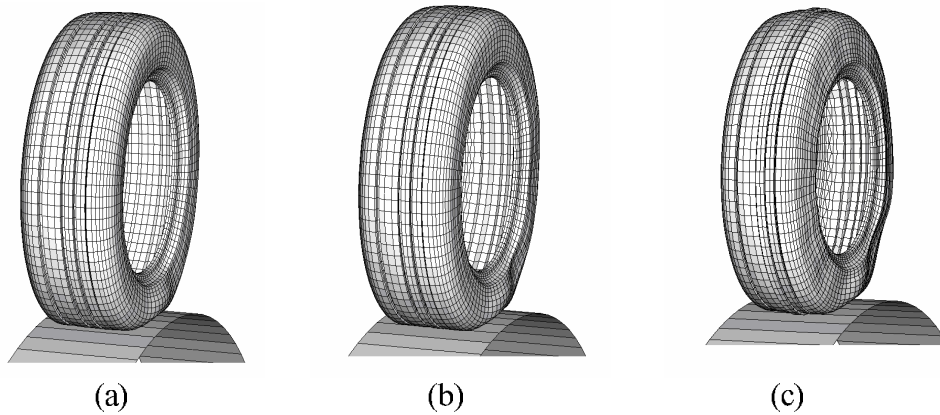


Figure 5: Simple model (type A). (a) 160km/h, (b) 205km/h, (c) 245km/h.

In Table 2, the critical speeds predicted by the finite element analyses are compared with those measured by an independent experiment, where the percentage values in parenthesis indicate the relative errors estimated with respect to the experimental results. Above all, one can figure out that the prediction accuracy of the patterned tire model is higher than the simple tire model, such that the maximum relative error is reduced by more than 50%. One interesting observation is that the critical speeds predicted by the simple tire model are vastly overestimated, which implies that the disregard of the detailed tread grooves results in a relative shear stiffness higher than the actual value of the real patterned tire. The overestimation of the critical speed when the tread grooves and blocks are ignored has been also presented in the paper by Togo [2]. Thus, it has been justified that the detailed tread

geometry should not be ignored to get a reliable prediction of the tire critical speed.

Table 2: Comparison of the critical speeds ($p_i = 137.9kPa$ and $F_y = 475kgf$)

Critical speed V_c (km/h)		
Numerical analysis		Experiment
Patterned tire model	Simple tire model	
182 (4.21%)	205 (7.89%)	190

Conclusion

A numerical technique for predicting the critical speed of tires has been introduced in this paper by utilizing the damped transient dynamic rolling analysis of 3-D patterned tire model. The overall stiffness, the total mass and the structural damping of the patterned tire were accurately reflected by fully taking the detailed tread geometry and the complex tire material composition into consideration. The verification experiment confirms the reliability of the proposed technique using 3-D patterned tire models such that the maximum relative error of the predicted critical speeds with respect to the experimental results is less than 5%, in contrast to the simple tire models.

References

1. Clark, S. K. (1981): *Mechanics of Pneumatic Tires*, U.S. Government Printing Offices.
2. Togo, K. (1964): "Standing wave on pneumatic tire at high speed", *Memoirs of the Defense Academy*, Vol. 4, No. 1, pp. 43-56.
3. Cho, J. R., Kim, K. W., Jeon, D. H. and Yoo, W. S. (2005): "Transient dynamic response analysis of 3-D patterned tire rolling over cleat", *European Journal of Mechanics A/Solids*, Vol. 24, pp. 519-531.
4. Cho, J. R., Kim, K. W., Yoo, W. S. and Hong, S. I. (2004): "Mesh generation considering detailed tread blocks for reliable 3-D tire analysis", *Journal of Advances in Engineering Software*, Vol. 35, pp. 105-113.
5. Chatterjee, A., Cusumano, J. P. and Zolock, J. D. (1999): "On contact-induced standing waves in rotating tires: experimental and theory", *Journal of Sound and Vibration*, Vol. 227, No. 5, pp. 1049-1081.